Dynamic transformation of a near alpha high-temperature titanium alloy during hot deformation

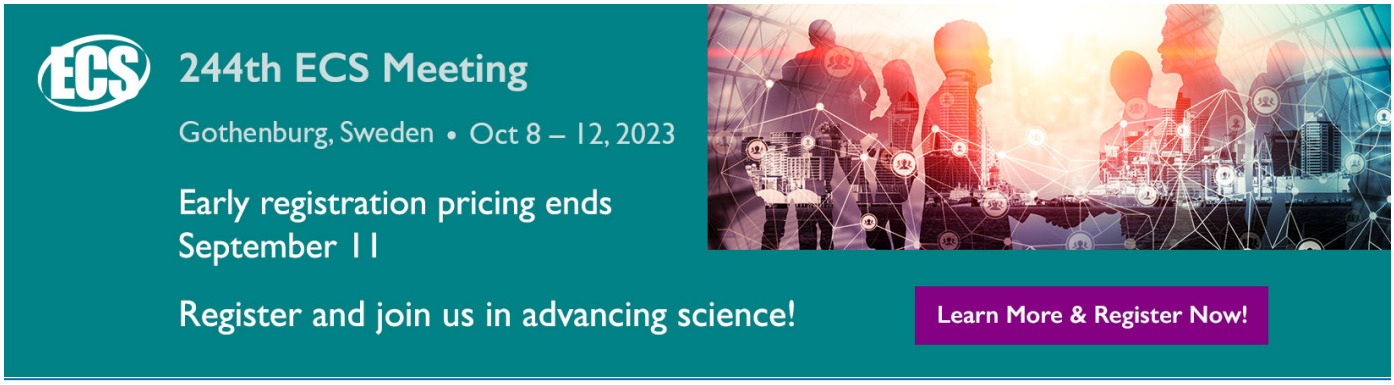

Dynamic transformation of a near alpha high-temperature titanium alloy during hot deformation

W X Xu, Z L Zhao*, N Liu, X Y Huang, S Li and Y B Wang
School of Materials Science and Engineering, Northwestern Polytechnical University, Xi'an 710072, P.R. China
*Corresponding author, E-mail address: zlzhao@nwpu.edu.cn

Abstract: The rapid drop of peak flow stress in the initial stage of hot compression experiment was found to be related to the occurrence of dynamic transformation from alpha phase (hcp) into beta phase (bcc) of a near α high-temperature titanium alloy. In order to predict the flow stress at all strain, the dynamic recovery (DRV) model and the Back-Error Propagation (BP) neural network architecture were established and comprehensively utilized to characterize the flow stress, which exhibited high accuracy in tracking the flow behavior at different deformation parameters. The variation of peak flow stress at initial stage of hot compression indicated that the rapid drop extent of peak value increased with the rise of deformation temperature, the decrease of strain rate and the increase of strain. It was worth noting that the dynamic transformation evolution in the microstructure exhibited the consistent variation of peak flow stress with different deformation parameters. The high-magnification microstructure analysis indicated that the dynamic transformation was accomplished by the immigration of α/β interface and the penetration of beta phase into alpha phase from edge to inside, all of which were related to the dislocation motion. The experimental result proved that the dynamic transformation was the dominant factor resulting in the rapid drop of peak flow stress at the initial stage of hot deformation.
Keywords.titanium alloy; hot deformation; dynamic transformation; microstructure evolution

1. Introduction

As an essential step for manufacturing most semi-finished and finished metal products, hot working process, such as forging, extrusion, rolling, etc., comprises the main approaches in the breakdown of primary coarse microstructure into fine and equiaxed microstructure[1, 2]. The most important goal of hot-working processes is that metals are deformed into the desired shapes under certain thermo-mechanical processing conditions to obtain appropriate microstructure with optimized mechanical properties. Rather the design of such processes relies heavily on the quantitative descriptions of plastic-flow constitutive behavior and microstructure evolution especially for titanium alloys as the limited hot workability and high microstructural sensitivity[3, 4]. During hot deformation, the work hardening tends to be counteracted by dynamic recovery (DRV) processes through the rearrangement and annihilation of dislocations, which results in steady state stress levels up to large strains for those metals and alloys with high stacking fault energy[5, 6]. When DRV weakened for those metals and alloys with low stacking fault energies, in which the flow softening phenomenon with a reduction in the flow stress value occurs with the strain increasing, usually as a result of the dynamic recrystallization (DRX) or the heat generation [7-11]. This kind of relatively widespread phenomenon was also observed in most of previous studied titanium alloys, such as near-α[2, 7, 12], α+β[13-15] and near-β titanium alloys[16, 17].

Therefore, it is indispensable to investigate the plastic-flow behavior and the microstructure evolution for determining the optimum hot deformation parameters.

Similar to the property of IMI834, Ti1100 and etc. high temperature titanium alloy [18], a near alpha high-temperature titanium alloy of Ti-5.8Al-4.8Sn-2Zr-1Mo-0.35Si-0.85Nd was developed as an engine material to work at the temperature up to 600˚C. Jia et al. found that the flow stress of Ti60 alloy decreases with increasing temperature and decreasing strain rate during the hot deformation, and formulated the constitutive equations to describe the dependence of the flow stress on deformation temperature and strain rate[19]. Peng et al. investigated that artificial neural network (ANN) model has a better prediction precision of the flow behavior in the hot compression for the as-cast Ti60 alloy [20]. Chen et al. studied the microstructure evolution of Ti60 alloy during hot deformation and revealed that the flow softening was mainly attributed to the globalization of the α lath at the strain rates of 0.01 s^{-1}and1 s^{-1} [21]. Above researches illustrated that the plastic-flow behavior and the microstructure evolution of Ti60 alloy during hot deformation is primarily understood, and provided theoretical foundation to determine the optimum hot deformation parameters. Recent research about Ti60 alloy illustrated that there was rapid dynamic transformation (DT) from α phase into β phase at low strain during hot deformation which could result in the drop of peak flow stress. Similar DT phenomenon occurred in Ti-5.5Al-1.5Fe, IMI-834 and C.P. Ti alloys during hot deformation [22, 23], and Jonas et al[24] found that the harder α phase with hexagonal close-packed (hcp) crystal structure transforms into softer β phase with body-centered cubic (bcc) crystal structure is responsible for the reduction of flow stress after the peak value. In order to comprehensively grasp the microstructure evolution behavior of the alloy during the hot deformation, the effect of DT from harder phase into softer phase on the flow softening of two-phase metals and alloys should be worthy of attention since the deformation-induced transformations of austenite to ferrite at temperatures above the Ae_3 could influence the flow behavior and microstructure morphology [25-28]. Based on the hot compression of Ti-5.8Al-4.8Sn-2Zr-1Mo-0.35Si-0.85Nd high temperature titanium alloy, the reason for the rapid decrease of peak stress at the low strain was analyzed. Additionally, the flow stress at all strains was accurately predicted by DRV and ANN model on the basis of the obtained hot compression data. Moreover, the volume fraction of DT from α phase to β phase at low strain was calculated according to the predicted flow stress data and the principle of stress balance. Finally, the microstructure evolution morphology of the alloy at low strain was observed, and the DT mechanism within microstructure was analyzed. In this paper, the relationship between the flow stress and microstructure evolution of the near α high temperature titanium alloy was illustrated, which was of great significance for optimizing the hot deformation parameters and microstructure morphology of the alloy.

2. Experimental procedures

The material used in this investigation was a high-temperature titanium alloy with chemical compositions (wt.%) of Al:6.14, Sn: 3.68, Zr: 3.43, Mo: 0.52, Si: 0.55, Ta: 0.96, Nb: 0.40, Ti: Bal. The β transus of this alloy was measured to be 1045˚C through metallographic observation method. Cylindrical specimens with a diameter of 8 mm and a height of 12 mm were machined from the as-received bar. The primary microstructure of the specimen displays the typical bimodal morphology which is mainly composed of equiaxed phase in a lamellar α+β matrix, as shown in figure1. Isothermal compression tests were carried out on a Gleebe-3500 thermomechanical simulator in deformation temperature range of 960-1050˚C and strain rate range of 0.001-10s^{-1} in vacuum environment. All specimens were heated to the desired temperature with a constant heating rate of 5˚C per second, holding for 5 min to eliminate the thermal gradient, and then compressed to the stated height. The specimens were immediately water quenched after compression to retain the high temperature deformation microstructure. In order to minimize the friction during hot deformation, the tantalum foil with the thickness of 0.1mm was used between the specimen and dies. The flow stress-strain curves were recorded automatically from load-stroke data in the isothermal compression experiments. The microstructure at the central region of hot compression specimens was observed by using the OLYMPUS GX-71 optical microscope, TESCAN VEGA 3 LMU scanning electron microscope and

Talos F200X high-resolution transmission electron microscopy.

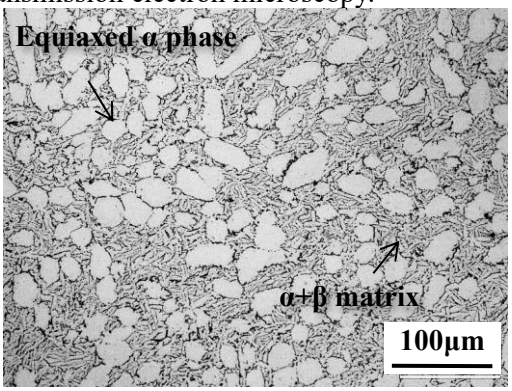

Figure 1. Primary bimodal microstructure of Ti-5.8Al-4.8Sn-2Zr-1Mo-0.35Si-0.85Nd alloy specimen.

3. Results and discussions

3.1. The rapid decrease of flow stress at low strain

The flow stress-strain curves of Ti-5.8Al-4.8Sn-2Zr-1Mo-0.35Si-0.85Nd alloy under different deformation temperatures and strain rates are shown in figure2. Almost at all compression curves, it can be found that the flow stress rapidly increases to a peak value at extremely small strain, then rapidly decreases，and gradually falls towards to a relatively steady state with increasing strain, exhibiting typical characteristics of initial work hardening followed by flow softening. Different deformation temperature and strain rate have great influence on the flow stress curve. At deformation temperature of 930°C and strain rate of $0.001s^{-1}$, the flow stress quickly reached the steady value at small strain. While the strain rate increased into $10s^{-1}$, the steady stress could be achieved only until reaching larger strain. Dissimilar strains of obtaining the steady stress suggest that the slower strain rate can provide enough time for DRV, DT and DRX to counteract the hardening behavior. The higher temperature is also beneficial to eliminate the hardening effect since the dislocation motion and recrystallization were enhanced due to the heat activation.

It is worth noting that the flow stress of the alloy will reach the peak and then decrease rapidly at the smaller strain (<0.05) during the hot compression process. In addition, the corresponding strain of rapid decrease will be very different with different deformation parameters. As seen from figure 2, the smaller the strain rate is at the same temperature, the smaller the strain corresponding to the rapid decline of peak stress is; the higher the temperature is, the smaller the strain corresponding to the rapid decline of peak stress is. Based on the characteristics of the flow stress curve, the flow stress could be divided into 3 periods including hardening, softening and equilibrium state. Without any doubt, the hardening effect was induced by the dramatically development of the dislocations at the initial stage of the plastic deformation. Normally, the flow softening of titanium alloy during the hot deformation is related to DRV, DRX, microstructure evolution and temperature rise as mentioned above. However, the flow softening effect due to DRV could only be in balance with work hardening and could not cause the stress drop. DRX and temperature rise could usually lead to the flow softening and stress drop at the large strain, while it is not possible to seriously reduce the flow stress at initial small strain less than 0.05. At present, it was found that the rapid decrease of peak stress at the smaller strain was mainly related to the dynamic phase transition [29].

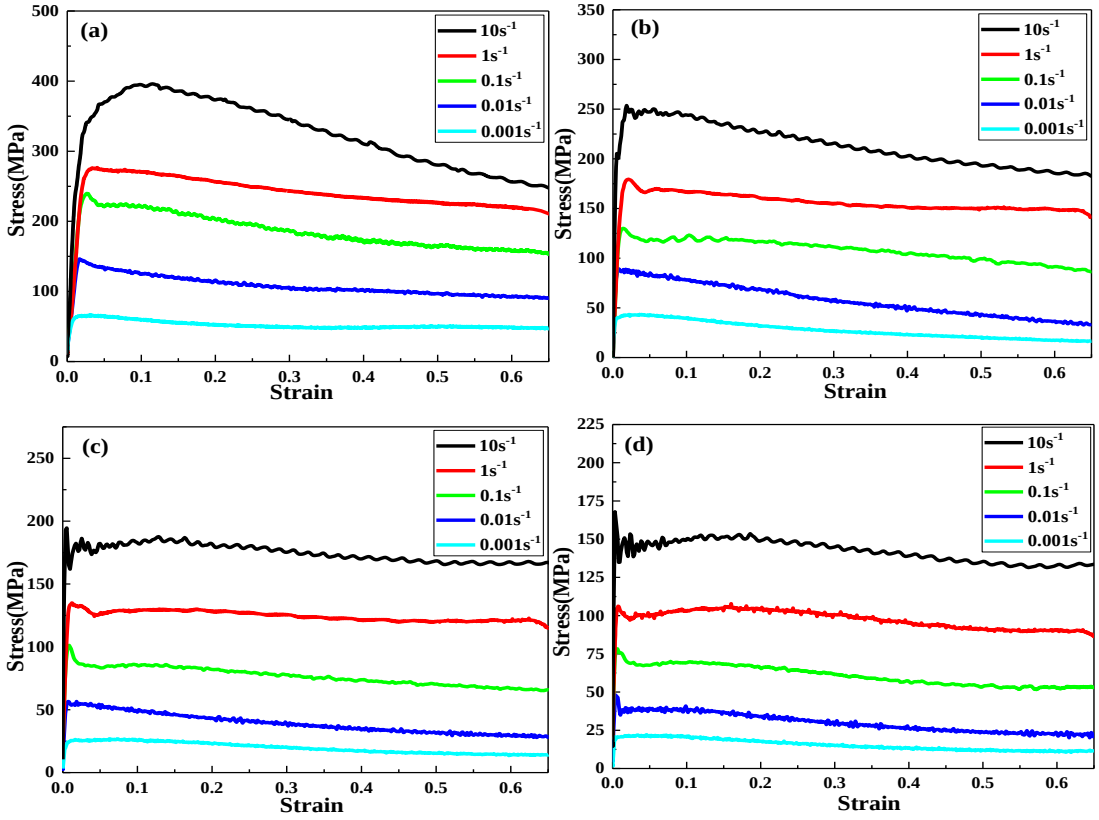

Figure 2. Flow stress-strain curves of Ti-5.8Al-4.8Sn-2Zr-1Mo-0.35Si-0.85Nd alloy at temperatures of 930°C (a), 960°C(b), 990°C(c) and 1020°C(d).

3.2. The modeling and prediction of flow stress

To further analyze the effect of DT on flow behavior, the flow curve of Ti-5.8Al-4.8Sn-2Zr-1Mo-0.35Si-0.85Nd alloy after peak value is considered to be the coefficient result of DRV, DT and DRX, as displayed in figure3. A similar method was used to analyze the process of flow softening phenomenon attributed to DRX, in which the stress–strain curve was considered to be the net result of the simultaneous operation of DRV and DRX [10, 30-33]. During hot deformation of Ti-5.8Al-4.8Sn-2Zr-1Mo-0.35Si-0.85Nd alloy, work hardening firstly increases the dislocation density to a relatively high level and leads to the rapid increase of flow stress. With the assumption that DT and DRX do not occur, work hardening would continuously lead the increase of stress to the saturated stress (σ_{sat}), and achieve an equilibrium state with the DRV, shown as the blue short dash dot line in figure 3. Once the critical stress of σ_c is reached, the softening effect of DT is initiated as the hardened α phase transforms into softer β phase(α→β) which results in the reduction of white α phase in the microstructure as indicated in figure 3. The flow stress peak (σ_p) represents the temporary balance between DT softening effect and work hardening effect is achieved. The further increase of strain accelerates the DT from α into β phase (the microstructure in figure 3), while the completion of the DT phenomenon just reduces the flow stress to an assumed stress (σ_{DT}) since the DRX is unlikely to occur or occurs to a very low degree at the smaller strain as shown in the red dash line. Therefore, the difference between the saturated stress and the experimental stress ($\Delta\sigma$) at the beginning of deformation can be identified as the net softening stress of DRV and DT. With the strain increasing, the occurrence of another softening process of DRX plays as the predominant flow softening mechanism at a critical strain of DRX (ε_{DRX}) which is larger or smaller than the termination strain of DT (ε_{DT}) depending on the deformation conditions.

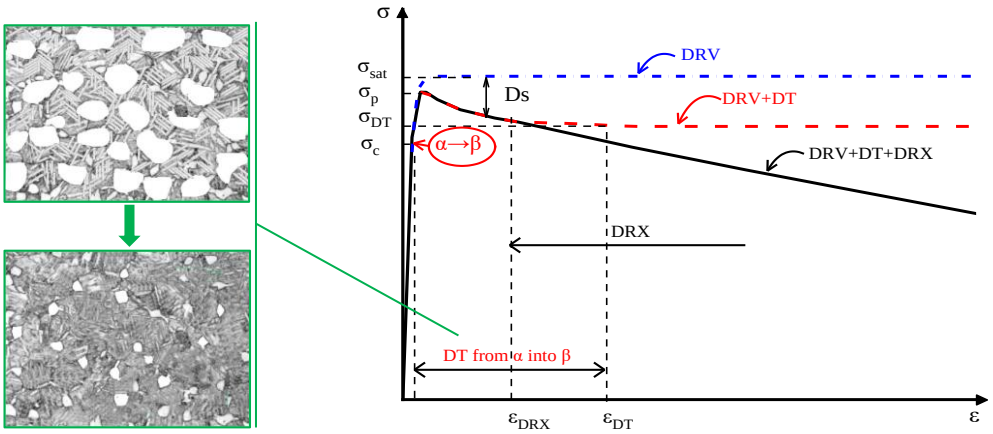

Figure 3. Schematic presentation of flow curves for DRV, DT and DRX of Ti-5.8Al-4.8Sn-2Zr-1Mo-0.35Si-0.85Nd alloy.

Considering the combining effect of the work hardening and DRV, Mecking and Kocks[34] proposed the expression about the average dislocation density $\boldsymbol{\rho}$ and the stress $\boldsymbol{\alpha}$ as following:

$$\sigma=\alpha Gb\rho^{1/2} \tag{1}$$

Where $\boldsymbol{\alpha}$ is the material parameter, $\boldsymbol{G}$ is the shear modulus, $\boldsymbol{b}$ is the burger vector. The relationship between the dislocation density and the strain during the deformation can be described as K-M model[34]:

$$d\rho / d\varepsilon = k_1\rho^{1/2} - k_2\rho \tag{2}$$

Where $d\rho/d\varepsilon$ is the rate that the dislocation density increases with the strain, $k_1\rho^{1/2}$ is the work hardening induced by the rapid dislocations increasing, $k_2\rho$ is the DRV softening effect resulted from the elimination and rearrangement of dislocations. The formula can also be expressed as:

$$-k_2 d\varepsilon / 2 = d\ln\left(k_1 - k_2\rho^{1/2}\right) \tag{3}$$

Integration of this formula can be written as:

$$\ln\left(k_1 - k_2\rho^{1/2}\right) = -k_2\varepsilon / 2 + C \tag{4}$$

When the material starts to yield, ε=0 and $\rho=\rho_0$, it can be deduced that $\exp C = k_1 - k_2\rho_0^{1/2}$. So

$$\rho^{1/2} = \frac{k_1}{k_2}\left[1-\exp\left(-k_2\varepsilon/2\right)\right] + \rho_0^{1/2}\exp\left(-k_2\,\varepsilon/2\right) \tag{5}$$

As $\boldsymbol{\rho}$ and $\boldsymbol{\rho_0}$ can be replaced by $\left(\sigma/\alpha Gb\right)^2$ and $\left(\sigma_0/\alpha Gb\right)^2$ respectively. Then the flow stress can be expressed with strain as following:

$$\sigma = \sigma_0\exp\left(-k_2\,\varepsilon/2\right) + \alpha Gb\frac{k_1}{k_2}\left[1-\exp\left(-k_2\,\varepsilon/2\right)\right] \tag{6}$$

When the strain tends to be infinite, $\sigma=\alpha Gb\left(k_1/k_2\right)$, here the saturated stress can be obtained. Therefore, the dynamic recovery model can be expressed as following:

$$\sigma=\sigma_{sat} - \left(\sigma_{sat} - \sigma_0\right)\exp\left(-k_2\,\varepsilon/2\right) \tag{7}$$

Where the value of $\boldsymbol{\sigma_0}$ can be achieved by the experimental flow stress directly. Then the saturated stress and material parameter are still unknown.

A concept of work hardening rate was proposed by Poliak and Jonas[35] as $\theta=d\rho/d\varepsilon$, which is used to determine the value of saturated stress $\boldsymbol{\sigma_{sat}}$. By conducting first - order partial derivatives on the stress-

strain curves, the relationship between the work hardening rate $\boldsymbol{\theta}$ and the stress $\boldsymbol{\sigma}$ can be plotted as figure 4. When σ=0, the increasing of the flow stress induced by the work hardening will stop and the dynamic softening happens. So, at this stress value, the first inflection point indicates the critical stress $\boldsymbol{\sigma_c}$ of dynamic softening. If the dynamic softening does not happen, then the flow stress will increase into a saturated stress, therefore, the $\boldsymbol{\sigma_{sat}}$ can be determined as the cross point of $\boldsymbol{\sigma}$ axis and the tangent extension at $\boldsymbol{\sigma_c}$.

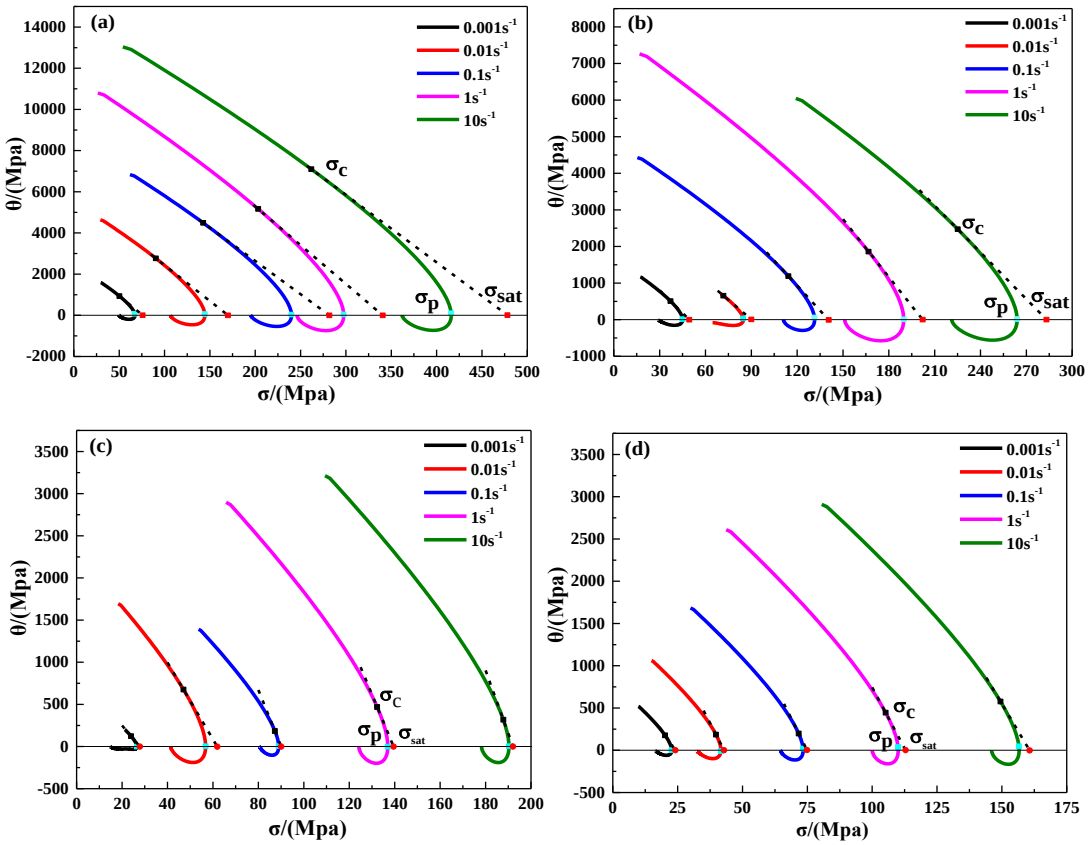

Figure 4. Relationship between the work-hardening rate (θ) and flow stress (σ) at temperatures of 930°C (a), 960°C(b), 990°C(c) and 1020°C(d).

The discrete data of saturated stress $\boldsymbol{\sigma_{sat}}$ and maximal stress $\boldsymbol{\sigma_p}$ were plotted in figure 5(a) which were fitted by linear function. It is obvious that the linear relationship between $\boldsymbol{\sigma_{sat}}$ and $\boldsymbol{\sigma_p}$ can be fitted as $\sigma_{sat}=1.145\sigma_p$. Similarly, the relationship between $\boldsymbol{\sigma_0}$ and $\boldsymbol{\sigma_p}$ can be fitted as a linear function $\sigma_0=0.832\sigma_p$, shown in figure 5(b).

Taking logarithm on the dynamic recovery model, it can be transferred into the following equation:

$$2\ln\left(\left(\sigma_{sat}-\sigma\right)/\left(\sigma_{sat}-\sigma_0\right)\right)=-k_2\varepsilon \tag{8}$$

It can be seen that $2\ln\left(\left(\sigma_{sat}-\sigma\right)/\left(\sigma_{sat}-\sigma_0\right)\right)$ and the strain $\boldsymbol{\varepsilon}$ can be fitted in a linear relationship to obtain the slop $\boldsymbol{-k_2}$. In the empirical formula[36] $k_2=A\dot{\varepsilon}^n\exp\left(-Q_{k_2}/RT\right)$, $\boldsymbol{A}$ and $\boldsymbol{n}$ are constants, Q_{k_2} is the activation energy of the material during the hot deformation (J/mol), $\boldsymbol{R}$ is the thermodynamic constant (8.314kJ/mol). By taking logarithm on above experience equation, it can be written as

$$\ln k_2=n\ln\dot{\varepsilon}-Q_{k_2}/RT+\ln A \tag{9}$$

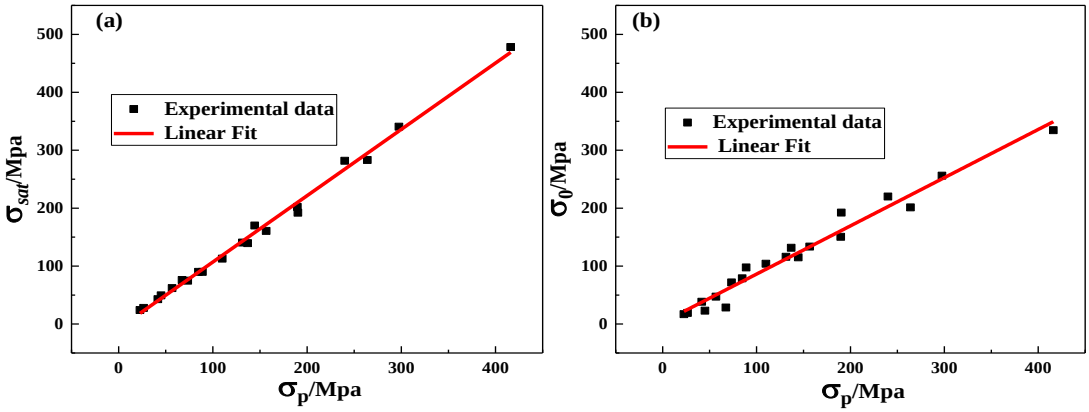

Figure 5. The linear relationship between steady state stress (σ_{sat}) (a), yield stress (σ_0) (b) and peak stress (σ_p).

By substituting the varying value under different conditions into equation 9, the value of $\ln k_2$ versus $\ln \dot{\varepsilon}$ and $1000/T$ can be calculated. According to the fitted linear relationship between $\ln k_2$ and $\ln \dot{\varepsilon}$, $1000/T$ respectively, the parameters of n, A, and Q_{k_2} can be obtained. Finally, the k_2 can be expressed with a function of temperature and strain rate as following:

$$k_2 = e^{29.05982}\dot{\varepsilon}^{-0.07929}\exp\left(-239611/RT\right) \tag{10}$$

According to the calculation and fitting above, the DRV model can be determined as:

$$\begin{cases} \sigma = \sigma_{sat} - \left(\sigma_{sat} - \sigma_0\right)\exp\left(-k_2\,\varepsilon/2\right) \\ \sigma_{sat} = 1.145\sigma_p \\ \sigma_0 = 0.832\sigma_p \\ k_2 = e^{29.05982}\dot{\varepsilon}^{-0.07929}\exp\left(-239611/RT\right) \end{cases} \tag{11}$$

The DRV model is able to express the flow stress at the initial deformation stage of Ti-5.8Al-4.8Sn-2Zr-1Mo-0.35Si-0.85Nd alloy, but fail to predict the stress varying during the whole process. Therefore, the method of ANN model was applied to reveal the constitutive relation during the mid-to-late period of the hot deformation. The standardized temperature, strain rate and strain were treated as input layer, while the stress was obtained by the output layer. As the effect of the input parameters were nonlinear on the stress, the tansig function was used to connect input and hidden layers[37]. The purelin function was used to transfer between hidden layers and the training function was selected as its fastest training rate and minimum error. The DRV model is suitable to predict the elastic and initial plastic deformation period and the ANN model tallies with the flow stress varying during the plastic deformation period. The combination of the DRV model and the ANN model provide the prediction for the flow stress at all strains during the deformation process as shown in figure 6. It is obviously that the prediction of the DRV model and the ANN model basically coincide with the experimental data.

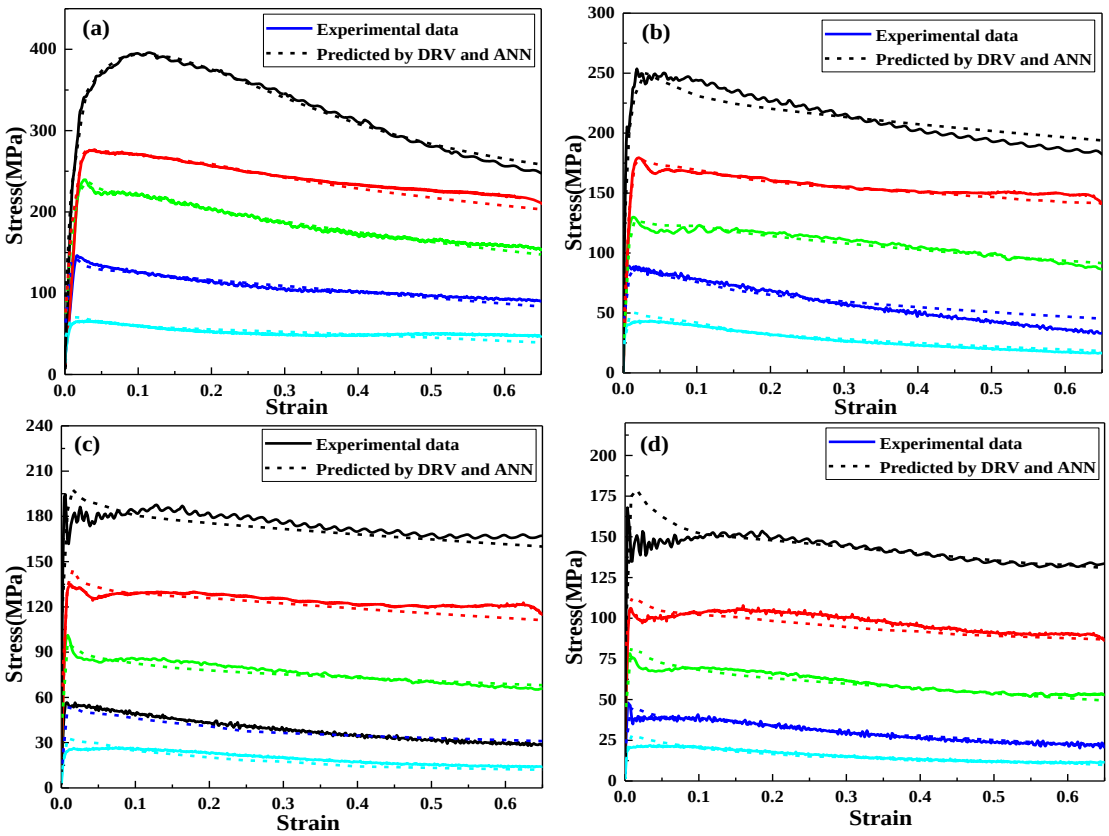

Figure 6. Comparison between the test and predicted flow stress at temperatures of 930°C (a), 960°C(b), 990°C(c) and 1020°C(d).

3.3. The effect of hot deformation parameters on DT

Figure 7 shows the microstructure of the alloy with the 10% compression at different temperature and strain rate of 0.001s^{-1}. Compared with the initial microstructure (figure 1), it can be found that the size of primary α phase in the microstructure after hot deformation decreases significantly and tends to be spherical, and the number of primary α phase decreases significantly with the increase of deformation temperature. According to the calculation results of DT in the above section, the volume fraction of α→β at the temperature of 930°C, 960°C, 990°C, 1020°C, the strain rate of 0.001s^{-1} and the compression of 10% is 13.5%, 32.7%, 64.5% and 95.6%, respectively. The α phase content in the initial microstructure in figure 1 is about 97%, and the residual α in the microstructure is calculated to be 83.9%, 65.3%, 34.4% and 4.3% respectively, which is basically consistent with the amount of residual α phase in the microstructure at corresponding deformation parameters in figure 7.

The effect of different temperatures on the microstructure when the alloy is only heated is shown in figure 8. Obviously, the heating and holding at different temperatures also have a great influence on the microstructure. However, compared with the microstructure heated at 930°C and held for 20min in figure 8(a), the size of primary α phase in the microstructure deformed after hot compression at 930°C decreases and the equiaxial effect is better in figure 7(a), and the number of α phase was larger. Compared with the microstructure heated at 990°C and held for 20min in figure 8(c), the size of primary α phase in the hot compression microstructure at 990°C in figure 8(d) significantly decreases to fine particles. It can be seen that the short-term hot deformation dramatically promotes the α→β phase transformation process in the microstructure of the alloy compared with the long-term hot deformation. The higher the deformation temperature is, the greater the content difference of primary α phase is, indicating that the promotion effect of hot deformation on α→β phase transformation will be enhanced at the higher temperature.

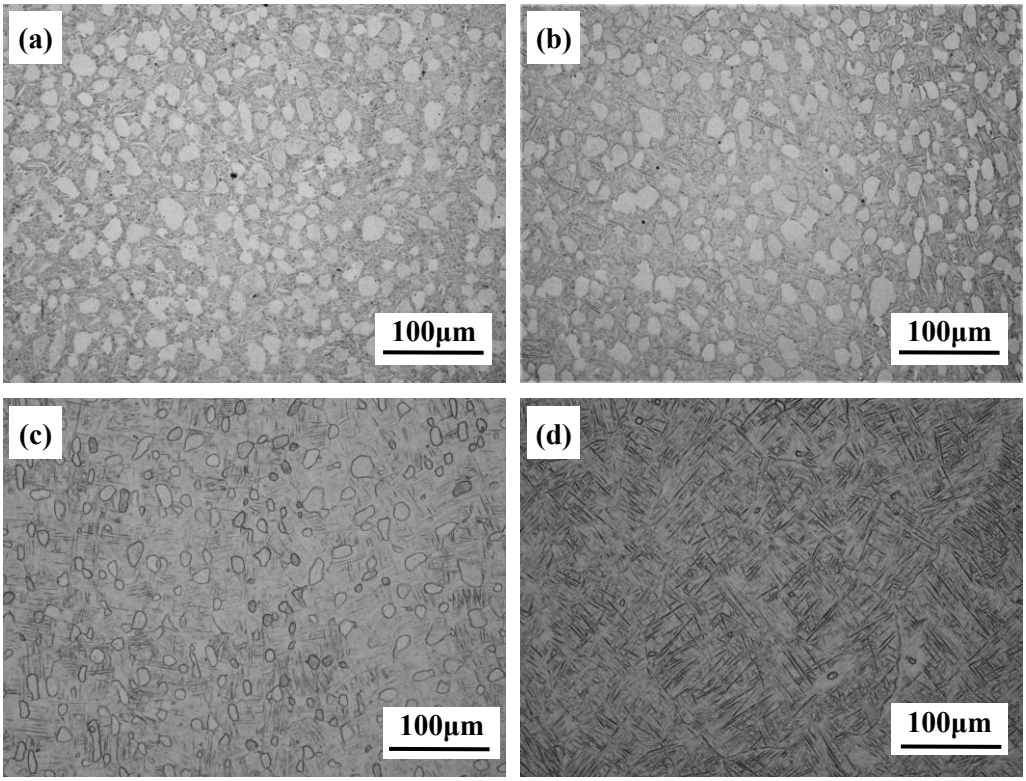

Figure 7. Microstructure compressed with strain rate of 0.001s^{-1}, deformation degree of 10% and temperatures of 930°C(a), 960°C(b), 990°C(c) and 1020°C(d).

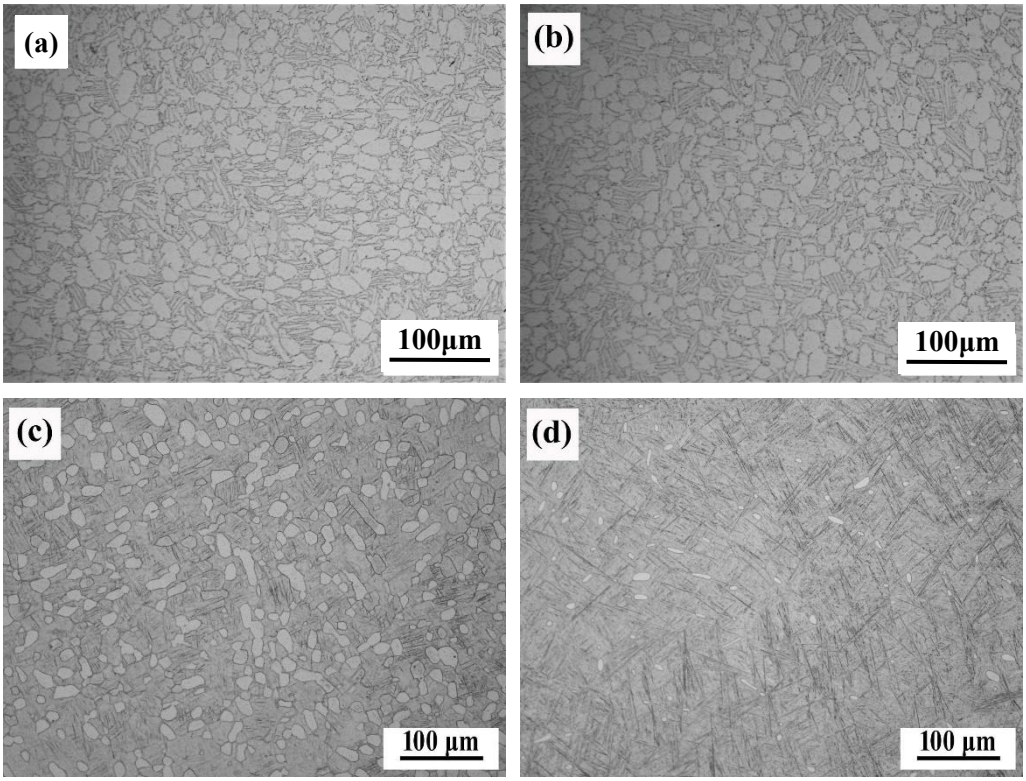

Figure 8. Microstructure heat-treated at 930°C(a), 960°C(b), 990°C(c) and 1020°C(d) for 20min.

It can be seen from figure 9 that the volume fraction of DT increases with the strain increasing, which is proved by the microstructure evolution during the deformation. As shown in figure 9, the secondary α particles shrunk and almost transformed into slate β as the deformation proceeded. The increase of strain could promote the DT at the low strain because the α→β phase transformation is a diffusion phase transformation, and the increase of strain could promote the generation of dislocation and other defects. Otherwise, the high density of dislocations provided diffusion path for the atoms, which is beneficial for the phase transformation.

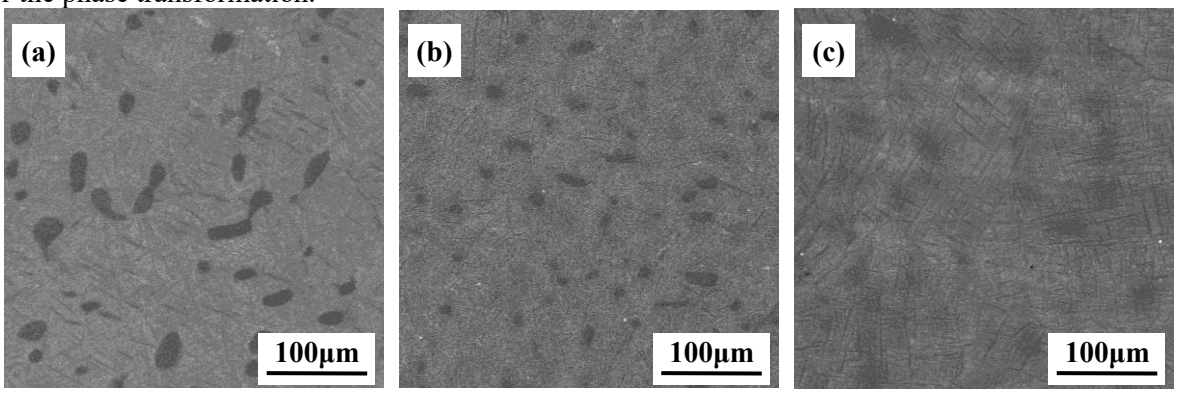

Figure 9. Microstructure after compression under temperature of 1020°C， strain rate of $0.1s^{-1}$ with strain of 5% (a), 10% (b) and 15% (c).

On the contrary, the volume fraction of DT decreases with the increasing strain rate according to the above calculations. The primary α particles shrunk and the secondary α particles dissolved obviously at lower strain rate. Figure 10 shows that the equiaxed primary α phase completely disappears at the temperature of 1020°C, the strain rate of $0.001s^{-1}$ and the compression of 10%. At the higher strain rate in figure 10 (b), the α/β phase boundaries and the fine primary α phase with the uniform distribution are more clearly observed. As the strain rate further increases, the α/β phase boundaries are unclear, while the number and size of the primary α phase are higher than those in the deformation microstructure at the lower strain rates. Otherwise, the primary α particles distributed more uniform when deformed at lower strain rate. This can be explained that the slow deformation provides enough time for the dislocation motion and atoms diffusion, which is beneficial to the phase transformation.

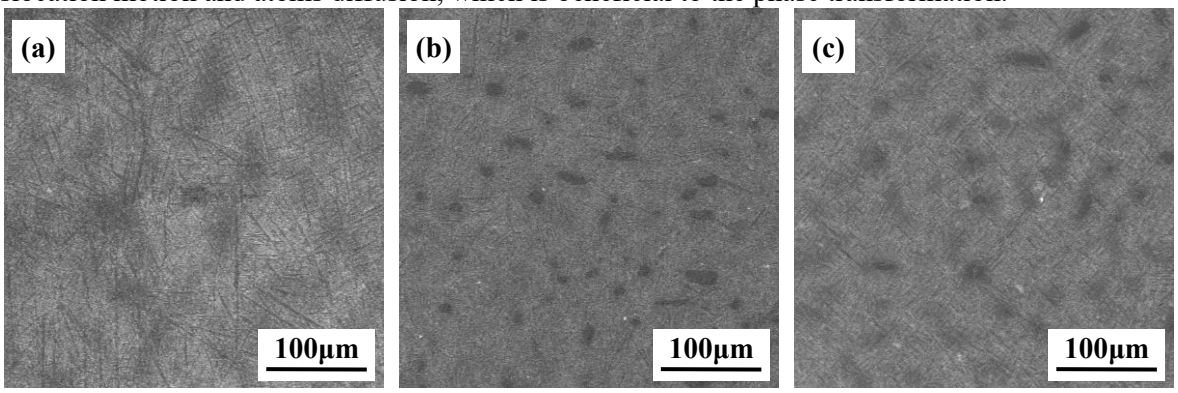

Figure 10. Microstructure after compression under temperature of 1020°C, deformation degree of 10% and strain rates of $0.001s^{-1}$ (a), $0.1s^{-1}$ (b) and $10s^{-1}$ (c).

The similar phenomenon of concurrent phase transformation was also observed in Ti-6Al-4V alloy[38] and Ti-6Al-2Sn-4Zr-6Mo alloy[39] during hot deformation, which further approves the significant effect of deformation parameters on the DT from α into β phase.

3.4. Mechanism of the DT

Figure 11 gives the typical SEM microstructures of Ti-5.8Al-4.8Sn-2Zr-1Mo-0.35Si-0.85Nd alloy compressed at strain rate of 0.001 s^{-1} and deformation temperature of 930~1020˚C. It can be found that the volume fraction and grain size of the primary equiaxed α phase changed markedly. When the deformation temperature increased from 930˚C to 990˚C (figure 11(a-c)), the volume fraction and grain size of the secondary lath α phase distributed around the primary α phase decreased and transformed into β phase. Under the action of the applied load, the harder α phase and the softer β phase deform in a coordinated manner. Then a substructure formed inside the primary α phase, as shown by the white arrow in figure 11(b), which provides favorable conditions for the α phase dissolving by a means of β phase penetrating α phase from the edge to the center. At 990℃, the primary α phase shrinks significantly and the boundaries are flatter due to the migration of the α/β interface, and the size of the residual secondary α phase also shrinks significantly. When the deformation temperature rises to 1020˚C, the α phases have completely transformed into the β phase, and more obvious β grain boundaries appear, as shown by the white dotted lines in the figure 11(d).

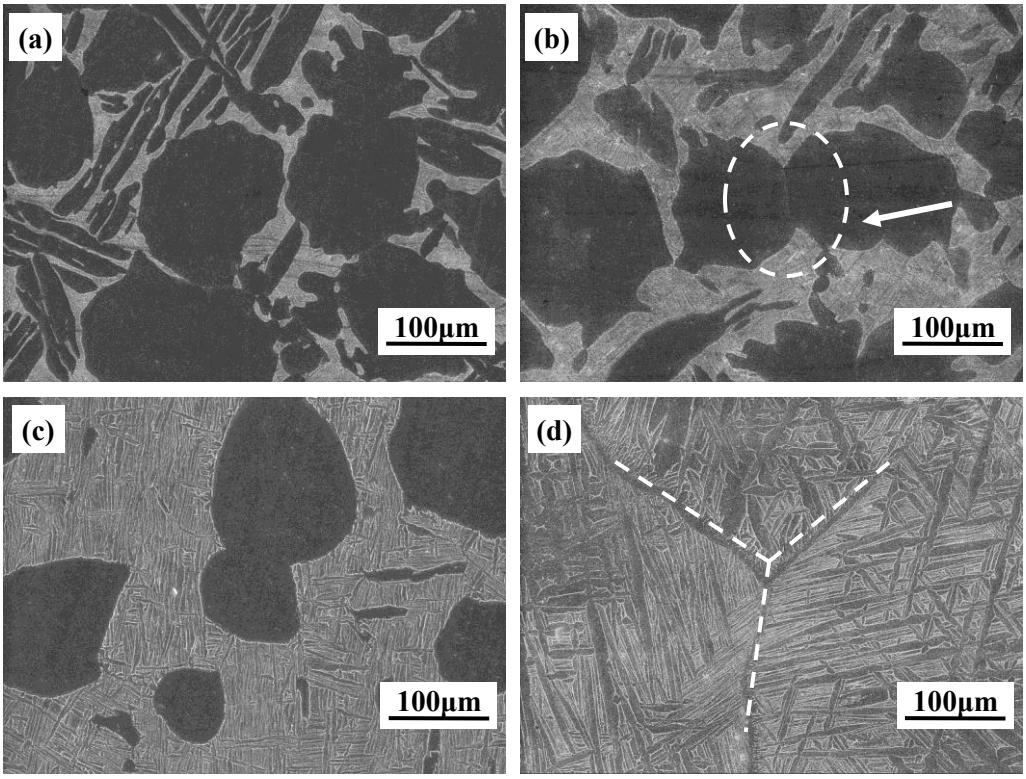

Figure 11. SEM microstructures under strain rate of 10 s^{-1}, deformation degree of 5% and deformation temperature of 930˚C (a), 960˚C (b), 990˚C (c), and 1020˚C (d).

It can be summarized that the α→β phase transformation of Ti-5.8Al-4.8Sn-2Zr-1Mo-0.35Si-0.85Nd alloy during hot deformation is mainly controlled by two ways. One is that the α phase shrinks continuously by the migration of α/β interface. The other is that the β phase penetrates the original α particles with the help of the substructures formed inside the primary α phase to promote the dissolving of α phase. It has been reported that the driving force for the phase transformation is deformation storage energy causing by the piling-up of dislocations[40]. These two transformation mechanisms of α→β phase could be distinctly observed in the microstructure (displayed in figure 12) at 990˚C, low deformation amount of 5% and low strain rate of 0.001s^{-1}.

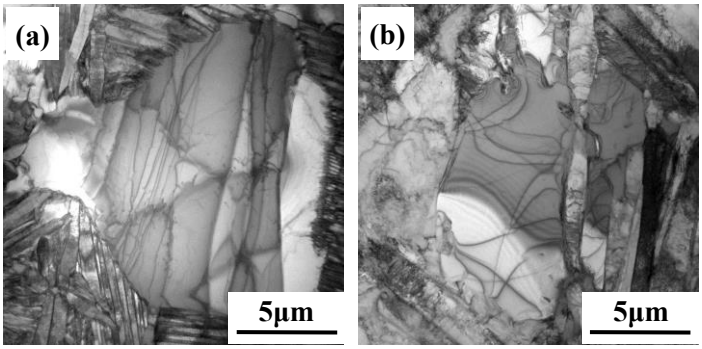

Figure 12. The homogeneous shrinkage of α phase (a) and direct penetration of β into α (b).

The immigration of α/β interface made the equiaxed α phase shrinking from the edge to the center, as shown in figure 11(a). The α/β phase interface could be clearly defined and the boundaries of primary α phase are flat. According to the literature[38], the α phase rotated in the circumferential direction to adapt to the external force, which was caused by the motion of dislocations. This can be proved by the TEM image in figure 13(a). The edges of α phase were entangled by large amount of dislocation segments, which made its orientation favorable conditions for the forming of surrounding β phases. When the DT from α to β phase occurred, the dislocations were consumed, resulting the rapid decreasing of the dislocation density. The α phase shrunk continuously by consequent rotation, maintaining an equiaxed shape, as shown in figure 13(b).

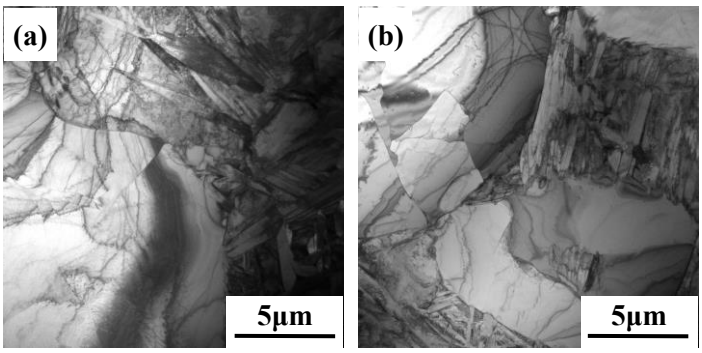

Figure 13. TEM microstructures with strain of 5% and strain rate of 0.001s^{-1}, under deformation temperature of 990˚C.

Furthermore, the β phase penetrated the α phase with the help of the substructure formed within the α phase as shown in figure 14. Generally, the α→β DT in this way occurs at high strain rates, which is different from the mechanism of α/β phase interface migration. The high strain rate caused a large number of dislocation proliferation during the hot deformation. As shown in figure 14, the mass dislocations existed in the interior and boundary of α and β phase. The high dislocation density not only effectively enhanced the high deformation storage energy, but also provided a suitable path for the penetration of β phase. Many substructures could be observed within α phase as shown in the arrows in figure 14, which are favorable for the α phase to be penetrated or even separated by β phase, resulting in the unclear α/β phase interface.

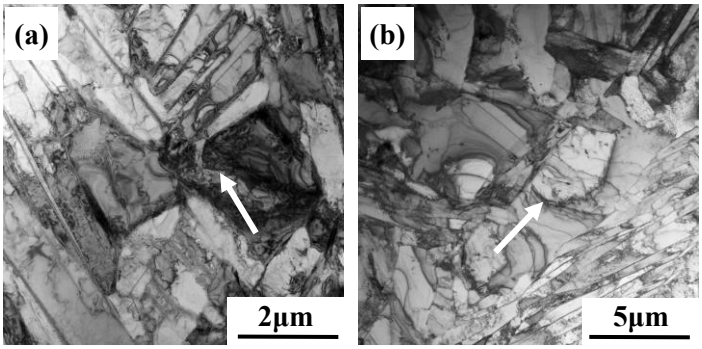

Figure 14. TEM microstructures with strain of 5% and strain rate of $10s^{-1}$, under deformation temperature of 990˚C (a), 1020˚C (b).

4. Conclusions

From the perspective of dynamic phase transformation, the reason for the rapid decrease of flow stress of a near α high temperature titanium alloy at low strain was revealed, and the volume fraction of dynamic phase transformation under different thermal deformation parameters was accurately predicted. Additionally, the mechanism of dynamic phase transformation was revealed. The flow softening phenomenon of Ti-5.8Al-4.8Sn-2Zr-1Mo-0.35Si-0.85Nd alloy at the initial period of the deformation was analyzed through introducing the occurrence of DT from α into β phase. The kinetic models of DT were developed to predict the volume fraction of DT from α phase into β phase at different temperatures and strain rates. The following conclusions can be drawn:

(1) The flow softening phenomenon of Ti-5.8Al-4.8Sn-2Zr-1Mo-0.35Si-0.85Nd alloy at the initial deformation stage is considered to be a result of the DT from α into β phase which is initiated by externally applied forces. The critical stress for the DT activation determined by transformation softening model is close to that calculated through double-differentiation method.

(2) Combing the thermodynamic equilibrium analysis of Ti-5.8Al-4.8Sn-2Zr-1Mo-0.35Si-0.85Nd alloy, the kinetic model expressed as a function of temperature, strain and strain rate is proposed to predict the volume fraction of DT.

(3) The predicted flow stress in accordance with the fitted experimental stress proves that the flow softening phenomenon at the beginning of hot deformation is mainly attributed to the occurrence of DT. The volume fraction of DT from α into β phase during hot deformation of Ti-5.8Al-4.8Sn-2Zr-1Mo-0.35Si-0.85Nd alloy could be accurately quantified by the proposed kinetic models.

(4) The volume fraction of DT from α into β phase is seriously influenced by the strain, strain rate and temperature. The deformation amount induces the occurrence of dynamic transformation and accelerates the phase transformation to achieve the thermodynamic equilibria. The low strain rate and high temperature are beneficial to the DT from α into β phase.

(5) The phase transformation of α to β phase of Ti-5.8Al-4.8Sn-2Zr-1Mo-0.35Si-0.85Nd alloy during hot deformation is mainly controlled by two ways. One is that the α phase shrinks continuously by the migration of α/β interface. The other one is that a substructure formed inside the primary α phase, which dissolved into β phase penetrating the original α particles.

References

[1] Semiatin S L, Seetharaman V and Weiss I 1998 *Mater. Sci. Eng. A* **243** 1-24
[2] Balasundar I, Raghu T and Kashyap P B 2014 *Mater. Sci. Eng. A* **600** 135-44
[3] Zong Y Y, Shan D B, Xu M and Lv Y 2009 *J. Mater. Process. Technol.* **209** 1988-94
[4] Li A B, Huang L J, Meng Q Y, Geng L and Cui X P 2009 *Mater. Des.* **30** 1625-31
[5] Lin Y C and Chen X M 2011 *Mater. Des.* **32** 1733-59
[6] Anand L 1985 *Int. J. Plast.* **1** 213-31
[7] Sun Z C, Yang H, Han G J and Fan X G 2010 *Mater. Sci. Eng. A* **527** 3464-71
[8] Liu J, Cui Z and Ruan L 2011 *Mater. Sci. Eng. A* **529** 300-10

[9] Lee B H, Reddy N S, Yeom J T and Chong S L 2007 *J. Mater. Process. Technol.* **187** 766-69
[10] Chen M S, Lin Y C and Ma X S 2012 *Mater. Sci. Eng. A* **556** 260-66
[11] Sun S D, Zong Y Y, Shan D B and Guo B 2010 *T. Nonferr. Metal. Soc.* **20** 2181-84
[12] Yang L, Wang B Y, Liu G, Zhao H J and Xiao W C 2015 *Mater. Des.* **85** 135-48
[13] Zhu Y C, Zeng W D, Liu J L, Zhao Y Q, Zhou Y G and Yu H Q 2012 *Mater. Des.* **33** 264-72
[14] Porntadawit J, Uthaisangsuk V and Choungthong P 2014 *Mater. Sci. Eng. A* **599** 212-22
[15] Lei L M, Huang X, Wang M M, Wang L Q, Qin J N and Lu S Q 2011 *Mater. Sci. Eng. A* **528** 8236-43
[16] Zhang J Q, Di H S, Wang H T, Mao K, Ma T J and Cao Y 2012 *J. Mater. Sci.* **47** 4000-11
[17] Li C, Zhang X Y, Li Z Y and Zhou K C 2013 *Mater. Sci. Eng. A* **573** 75-83
[18] Balasundar I, Raghu T and Kashyap B P 2013 *Prog. Nat. Sci. Mater. Int.* **23** 598-607
[19] Jia W J, Zeng W D, Zhou Y G, Liu J R and Wang Q J 2011 *Mater. Sci. Eng. A* **528** 4068-74
[20] Peng W W, Zeng W D, Wang Q J and Yu H Q 2013 *Mater. Des.* **51** 95-104
[21] Chen W, Zeng W D, Xu J W, Zhou D D, Wang S M and He S D 2019 J. *Alloys Compd.* **792** 389-98
[22] Koike J, Shlmoyama Y and Ohnuma I 2000 *Acta Mater.* **48** 2059-69
[23] Ding R, Guo Z X and Wilson A 2002 *Mater. Sci. Eng. A* **327** 233-45
[24] Jonas J J, Aranas C, Fall A and Jahazi M 2016 *Mater. Des.* **113** 305-10
[25] Yoshikazu M and Hiroshi Y 2006 *ISIJ Int.* **27** 492-8
[26] Yada H, Li C M and Yamagata H 2000 *ISIJ Int.* **40** 200-6
[27] Sun L, Muszka K, Wynne B P and Palmiere E J 2014 *Acta Mater.* **66** 132-49
[28] Ghosh C, Aranas C and Jonas J J 2016 *Prog. Mater. Sci.* **82** 151-233
[29] Zhao Z L, Liu N, Xu W X, Cao L C, Li S and Huang X Y 2021 *Mater. Lett.* **305** 130837
[30] Zahiri S H, Davies C and Hodgson P D 2005 *Scr. Mater.* **52** 299-304
[31] Quan G Z, Wu D S, Luo G C, Xia Y F, Zhou J, Liu Q and Gao L 2014 *Mater. Sci. Eng. A* **589** 23-33
[32] Jonas J J, Quelennec X, Jiang L and Martin É 2009 *Acta Mater.* **57** 2748-56
[33] Zong Y Y, Huang S, Wang Y and Shan D B 2014 *Int. J. Hydrog. Energy* **39** 3498-504
[34] Mecking H and Kocks U F 1981 *Acta Metall.* **29** 1865-75
[35] Poliak E I and Jonas J J 1996 Acta Mater. **44** 127-36
[36] Ye H B, Pan Q L, Chen Q, Zahng Z Y, Liu X Y and Li W B 2012 *T. Nonferr. Metal. Soc.* **22** 246-54
[37] Xue J, Lv Y, Qi S, Jiang S, Zhang X and Yun R 2014 *Lubr. Eng.* **39** 14-18
[38] He L J, Dehghan-Manshadi A and Dippenaar R J 2012 *Mater. Sci. Eng. A* **549** 163-7
[39] Dehghan-Manshadi A and Dippenaar R J 2012 *Mater. Sci. Eng. A* **552** 451-6
[40] Li L, Li M Q and Luo J 2015 *Mater. Sci. Eng. A* **628** 11-20

Acknowledgements
This study was financially supported by the National Natural Science Foundation of China (No. 51974259) and Xi'an Science and Technology Bureau Project (No. 21ZCZZHXJS-QCY6-0008).